Hierarchical Proactive Control Based Grid-Forming Energy Router for Industrial Microgrid

Zixuan Zheng, *Member, IEEE*, Shijie Li, Chunjun Huang, *Member, IEEE*, Yunzhu Chen, Junhao Ma, Mingshun Zhang, Xianyong Xiao, *Senior Member, IEEE*, Jie Ren, and Qiang Fu, *Member, IEEE*

***Abstract*—Energy routers present a viable option for harvesting renewable energy sources (RESs) and ensure dependable electricity provision in industrial microgrids. This paper presents a multi-functional, grid-forming energy router (GFMER), accompanied by a hierarchical proactive control approach. The lower-layer controller handles the coordination strategies among photovoltaic (PV) systems, battery energy storage units (BESU), and DC/AC converters. In this layer, an optimized multi-objective droop control mechanism is presented to proactively regulate AC grid-side voltage imbalances and deviations. Meanwhile, the upper-layer control is deployed to maintain the DC bus voltage, and a novel power allocation module has been designed to enhance the dynamic transient support for grids. The effectiveness and practical value of this proposed methodology have been validated through MATLAB/Simulink and hardware-in-the-loop (HIL) experiments.**

***Index Terms*—Droop control, energy router, grid-forming, hierarchical control, proactive support.**

I. Introduction

With the acceleration of the global energy transition process, the proportion of renewable energy sources (RESs) in industrial microgrid continues to increase [1], [2]. However, power electronic equipment of RESs lacks the physical rotating shaft of the synchronous machine, which makes the new power system gradually show the characteristics of low inertia, weak damping and low short-circuit ratio, weaking the ability to form grid and to operate stably [3]. Power quality issues such as voltage sag, swell, and imbalance become notably significant in industrial microgrid contexts due to the critical operational needs of sensitive equipment, the direct impact on productivity and safety, potential cost implications from downtime, and the necessity to comply with stringent regulatory standards. In this context, the capability to provide dynamic support, which involves the rapid and flexible adjustment of active and reactive power outputs in response to changing grid conditions, becomes critical to ensuring reliable operation and high power quality under varying grid conditions. Hence, inverters connected to RESs are expected to form the grid and provide certain ancillary services such as proactive and dynamic support to meet the premium power supply for sensitive loads [4].

For high-quality operation and flexible regulation of power in microgrids, the concept of energy router (ER) was proposed, which has the characteristics of power conversion, energy management, and plug-and-play [5]. An ER is composed of a series of controlled components, which can be used as the intelligent interfaces of RESs, energy storage units, power grids, loads and other equipment. Compared with conventional multi-converter architectures, the integrated ER can achieve multi-level distribution and controllable flow of power with reduced component count, size, cost and power loss [6], [7]. The unique features and capabilities of ERs make them well-suited for forming and supporting modern grids characterized by increasing renewable energy penetration, and decentralized generation. Current research on ER predominantly concentrates on their structural design and energy management strategies [6], [8], [9], [10], [11], with limited investigation into their ability to provide proactive and dynamic grid support.

In addition, there are some studies exploring the dynamic support capability of RESs for power grids. Conventionally, proactive support from RESs is achieved by means of controlling the output current of the grid-connected converter, whose phase is synchronized with the grid by using phase locked-loop, meanwhile a current loop ensures power injection accuracy and current quality issues. A single-phase grid-connected strategy for photovoltaic (PV) with independent control of active and reactive power flow is discussed in [12]. In [13] and [14], a strategy for proactive support from PV inverters is proposed, which obtains the reference currents by calculating the power of the support. In [15], positive and negative sequence reference currents are calculated separately for proactive support under unbalanced faults. In [16], a reference current generator capable of eliminating active power oscillations and compensating voltage imbalances is proposed. However, the above proactive support strategy is applicable solely to grid-following control but not to grid-forming control, which lacks phase-locked loop. Droop control is a typical grid-forming control strategy with the advantage of quick control response. It has also been studied in

Received 15 April 2024; revised 22 October 2024 and 9 December 2024; accepted 22 December 2024. Date of publication 26 December 2024; date of current version 22 August 2025. This work was supported by Chengdu Municipal Science and Technology Program under Grant 2024-YF05-00653-SN. Paper no. TEC-00399-2024. *(Corresponding author: Xianyong Xiao.)*

Zixuan Zheng, Shijie Li, Yunzhu Chen, Junhao Ma, Mingshun Zhang, Xianyong Xiao, Jie Ren, and Qiang Fu are with the College of Electrical Engineering, Sichuan University, Chengdu 610065, China (e-mail: scuzzx@163.com; 17307244897@163.com; 1159228002@qq.com; mjh030124@163.com; mszhang@stu.scu.edu.cn; xiaoxianyong@163.com; renjieholmesjay@163.com; fuqiang346@qq.com).

Chunjun Huang is with the Department of Electrical Sustainable Energy, Delft University of Technology, 2628 CD Delft, The Netherlands (e-mail: c.j.huang@tudelft.nl).

Color versions of one or more figures in this article are available at https://doi.org/10.1109/TEC.2024.3522401.

Digital Object Identifier 10.1109/TEC.2024.3522401

the field of proactive support for power grids. A proactive support strategy based on hierarchical droop control is investigated in [17]. The secondary control mainly performs positive and negative sequence power calculations under voltage sags and sends voltage support signals to the primary control. Nevertheless, the experimental results show that the power quality control strategies for inverters are not accurate, leading to cause voltage deviations even when inverters support the grid. Reference [18] introduces a hybrid control strategy that merges frequency droop with a passivity-based switching function. Implementing this strategy allows the injection of positive/negative sequence active/reactive power to restore voltage levels. However, the simulation and experimental settings have a voltage sag depth of only 20%, which does not represent the supportive impact on more extreme cases. Prior investigations primarily concentrate on the control of inverters, with insufficient consideration for the system connected to the DC side of the inverter, which can precipitate oscillations in DC bus voltage. Moreover, the inverter capacity has not been adequately addressed.

Several studies have empowered ER with the capability to enhance power grid quality. In [19], an ER with five ports is presented, capable of integrating photovoltaic (PV) systems, energy storage, and both AC and DC loads. It features advanced energy management strategies that improve the power quality of the grid. However, the improvement in power quality is achieved by isolating fluctuations from loads and PV away from the grid, reducing potential disturbance sources but not actively reinforcing the grid's stability. In [20], the proposed ER can correct harmonics and ensure three-phase power balance in a microgrid. Yet, it does not provide voltage support during faults. In summary, current ER models are not designed to form and actively support the grid simultaneously, and the research addressing control of proactive support the grid is subject to certain limitations.

To address these issues, we propose a grid-forming, multi-functional energy router (GFMER) that features a hierarchical cooperative control scheme. This advanced GFMER is designed not only to establish and reinforce the grid but also to guarantee both the reliability and quality of power supply to loads. The significant benefits of our approach are summarized below.

1) The proposed GFMER provides multi-port access to the grid, battery energy storage unit (BESU), PV and loads. A comprehensive hierarchical control framework is developed, which integrates multiple operating modes—grid-connected, transient support, and grid-forming—within a unified energy router system.
2) Within the lower-layer controller, an improved multi-objective droop control is proposed that dynamically adjusts the positive and negative sequence reference power at multiple GFMERs to support the grid voltage in all operating modes.
3) A power allocation module is deployed in the upper-layer controller. It improves the dynamic support capability of the GFMER to the grid during grid-connected and transient support modes.

The rest of the paper is organized as follows. Section II introduces the basic topology of the GFMER. Section III shows the lower-layer controller while the upper-layer controller is provided in Section IV. Section V demonstrates experimental results. Finally, this article concludes in Section VI.

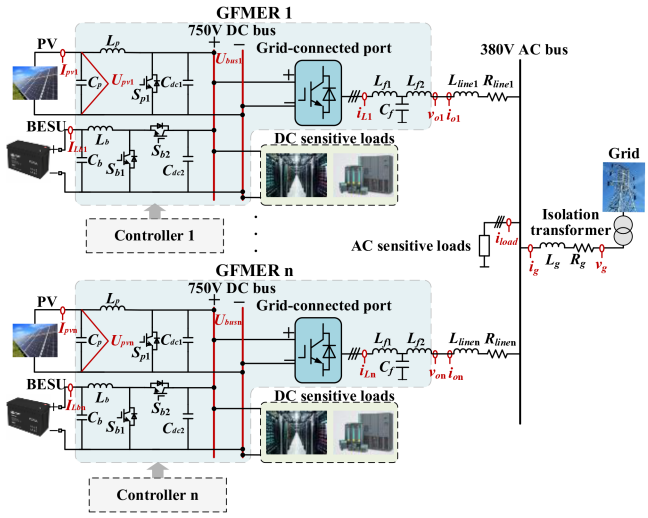

Fig. 1. Basic topology of the GFMER.

II. Basic Topology of the GFMER

The structure of a parallel connected GFMER system is shown in Fig. 1. Each GFMER is designed to 4 ports including:

1) *PV port:* In order to harvest renewable energy sources, the PV system is connected to the 750 V DC bus through a boost DC/DC converter.
2) *BESU port:* The BESU is crucial within the GFMER, serving to stabilize energy fluctuations resulting from load and power supply variations and providing backup when renewable energy is insufficient. To maintain energy balance between the DC and AC sides of the GFMER, the BESU is linked to the 750 V DC bus via a boost-buck bidirectional DC/DC converter.
3) *DC load port:* The DC load port is directly connected to the 750 V DC bus to meet the power demand of DC sensitive loads and adhere to voltage level standards specified in IEC 60038 [21].
4) *Grid-connected port:* The grid-connected port is an important part of the GFMER, facilitating connection between the energy router and the power grid for power transmission and proactive grid support. Furthermore, during severe grid faults, the energy router can be isolated by disconnecting this port.

Among the system, U_{bus1} and U_{busn} are the DC bus voltages of the *1*th and *n*th GFMER. I_{pv1}, I_{pvn} are the output current of PV in *1*th and *n*th GFMER, and U_{pv} is the output voltage of PV. I_{Lb1} and I_{Lbn} are the output currents of BESU in *1*th and *n*th GFMER. The grid-connected converter consists of a three-phase voltage source SPWM inverter and filter. In addition, R_g, L_g are the resistance and inductance of grid impedance. R_{linen}, L_{linen} are the line resistance and inductance of *n*th GFMER. u_g is the utility grid voltage. v_{o1} and v_{on} are the output voltages of *1*th

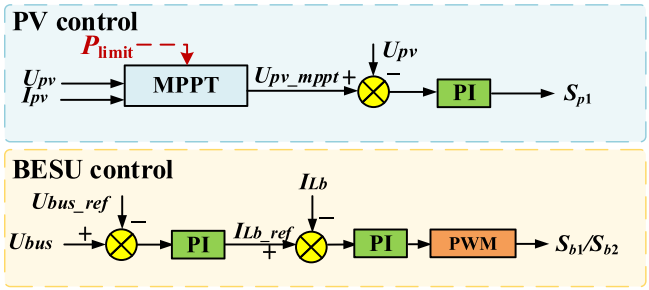

Fig. 2. Control strategy of PV and BESU.

and *n*th GFMER. i_{o1}, i_{on}, i_g, and i_{load} are the output current of *1*th and *n*th GFMER, the injected grid current, and the load current. 380 V AC sensitive load is the local load, which can be resistive, inductive, capacitive, and linear or nonlinear load.

The relationship among the injected grid current, the output currents of GFMER and the load current is:

$$i_g = i_{o1} + \cdots + i_{on} - i_{load} \tag{1}$$

Since the GFMER studied in this paper is connected to the 380 V/50 Hz low-voltage distribution network, the main circuit does not need to be electrically isolated, and the voltage level and electrical energy form are transformed by power electronic converters. The integrated full power electronic circuit contributes to the modularity and miniaturization of the GFMER [10].

III. The Lower-Layer Controller

The proposed hierarchical control strategy for the GFMER is organized into two distinct layers. The lower-layer controller system adopts a decentralized structure, with control modules specifically designed to meet varying operational objectives. These include control strategies for the PV, BESU, and DC/AC converter, optimized for its unique functional requirements. The details of these control techniques are elaborated in the following sections.

A. PV and BESU Control Strategy

The control mode of the PV port is designed to maximize the utilization of renewable energy power. Hence, the PV system employs maximum power point tracking (MPPT) control as its sole control strategy, as shown in Fig. 2. The conductance increment method is employed to achieve maximum power tracking, with an additional power limit (P_{limit}) imposed [22]. When the maximum output power of the PV system (P_{pv_mppt}) exceeds P_{limit}, the PV output power is capped at P_{limit}.

For the BESU, the constant voltage (CV) control strategy is adopted to ensure the precise stability of the DC bus voltage, as shown in Fig. 2. The CV control employs a double-loop strategy, consisting of an outer voltage loop and an inner current loop. The BESU reference output current can be calculated as:

$$I_{Lb\_ref} = k_{pb}(U_{bus} - U_{bus\_ref}) + k_{ib}\int (U_{bus} - U_{bus\_ref})dt \tag{2}$$

where k_{pb} and k_{ib} are the proportional and integral gains of the voltage loop PI controller.

B. Control Strategy of DC/AC Converter

Droop control is a method to control converter by simulating droop external characteristic curve of synchronous generator. To fulfill the requirements of self-regulation, communication independence, and grid-forming capability, the DC/AC converter adopts droop control. Additionally, industrial microgrids face significant challenges in maintaining reliable operation under voltage sags and imbalances. Dynamic support capability is essential to ensure reliable operation and high power quality under these varying conditions. It should be noted that not only positive sequence active/reactive power, but also negative sequence active/reactive power is needed to support the voltage at point of common coupling (PCC) under voltage sags [17], [18]. Hence, aim to meet the dynamic support needs of the power grid, an improved droop control based on positive and negative sequence separation is proposed which consists of primary control module and power calculation module.

1) Primary Control Module: During asymmetric faults, the voltage and current at PCC can be expressed as the sum of positive, negative and zero sequence components [23], [24]:

$$\begin{bmatrix} F_a \\ F_b \\ F_c \end{bmatrix} = \begin{bmatrix} F_a^+ \\ F_b^+ \\ F_c^+ \end{bmatrix} + \begin{bmatrix} F_a^- \\ F_b^- \\ F_c^- \end{bmatrix} + \begin{bmatrix} F_a^0 \\ F_b^0 \\ F_c^0 \end{bmatrix} \tag{3}$$

For a three-phase three-wire system, the zero-sequence component is negligible because the neutral point is not grounded.

The primary control module includes current inner loop, voltage outer loop, and droop control loop. These control loops are implemented in two-phase rotating reference frame (*d*-*q*) to facilitate decoupling. In addition, in order to filter out power ripples and improve control accuracy, active and reactive power are calculated and passed through first-order low-pass filters. It should be noted that the decoupling of positive and negative sequence is based on double second order generalized integrator (DSOGI), which has high precision, high reliability and excellent anti-interference ability [25].

The traditional droop control method is developed based on inductive line impedance, which may not align with the resistive impedance often encountered in low-voltage distribution networks [26]. This discrepancy can lead to active-reactive power coupling issues. To solve this problem, a virtual impedance is implemented to enhance the power sharing accuracy among the GFMERs, and also to make the system more damped without sacrificing system efficiency [27].

In addition, in order to reduce the frequency and amplitude deviation of the output voltage at the port, a secondary amplitude and frequency control is integrated with droop control. This control mechanism elevates the droop curve and operating point, restoring the voltage frequency and amplitude to nominal values while maintaining constant active and reactive outputs [28]. The schematic diagram is shown in Fig. 3. The grid-connected pre-synchronization control is implemented to enable the GFMER to operate seamlessly in both grid-connected and

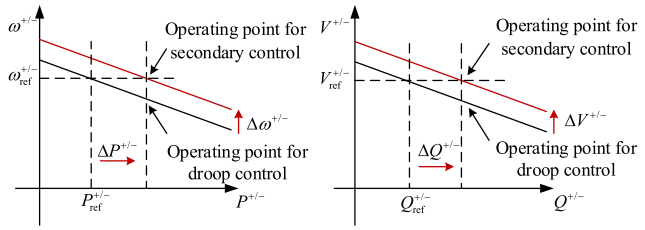

Fig. 3. The schematic diagram of secondary control.

off-grid modes, facilitating smoother transitions between these operational states. This pre-synchronization control utilizes voltage magnitude and phase difference as feedback signals, adjusted by proportional-integral (PI) controllers to generate compensation signals for converter voltage and frequency.

In summary, the proposed droop control after adding secondary control, virtual impedance and grid-connected pre-synchronization is expressed as follows:

$$\begin{aligned}\omega^{+/-} &= \omega_{ref}^{+/-} - k_p^{+/-}\left(P^{+/-} - P_{ref}^{+/-}\right) \\ &+ \left(k_{fp}^{+/-} + \frac{k_{fi}^{+/-}}{s}\right)\Delta\omega^{+/-} \\ &+ \left(k_{p1}^{+/-} + \frac{k_{i1}^{+/-}}{s}\right)\Delta\omega_{mg}^{+/-} \end{aligned} \tag{4}$$

$$\begin{aligned}V_{odref}^{+/-} &= V_{ref}^{+/-} - k_q^{+/-}\left(Q^{+/-} - Q_{ref}^{+/-}\right) \\ &+ \left(k_{Vp}^{+/-} + \frac{k_{Vi}^{+/-}}{s}\right)\Delta V^{+/-} \\ &+ \left(k_{p2}^{+/-} + \frac{k_{i2}^{+/-}}{s}\right)\Delta V_{mg}^{+/-} \\ &- \left(R_v^{+/-} i_{od}^{+/-} - X_v^{+/-} i_{oq}^{+/-}\right) \end{aligned} \tag{5}$$

$$V_{oqref}^{+/-} = 0 - \left(R_v^{+/-} i_{oq}^{+/-} - X_v^{+/-} i_{od}^{+/-}\right) \tag{6}$$

where $P_{ref}^{+/-}$ and $Q_{ref}^{+/-}$ are the positive/negative sequence active/reactive reference power respectively, which will be calculated in detail in the next section; $\omega_{ref}^{+/-}$ are the rated positive/negative sequence angular frequency; the parameters $k_p^{+/-}$ and $k_q^{+/-}$ are the positive/negative sequence active-frequency and reactive-voltage droop coefficients respectively; $R_v^{+/-}$ and $X_v^{+/-}$ are the virtual resistance and reactance respectively; $\Delta\omega^{+/-}$ and $\Delta V^{+/-}$ are the positive/negative sequence voltage angular frequency and magnitude difference respectively between the detected value and the reference value; $\Delta V_{mg}^{+/-}$, $\Delta\omega_{mg}^{+/-}$ are the positive/negative sequence voltage magnitude and phase difference respectively between the GFMER output value and the grid value. $\Delta\omega^{+/-}$ $\Delta V^{+/-}$ $\Delta V_{mg}^{+/-}$ and $\Delta\omega_{mg}^{+/-}$ can be calculated as:

$$\Delta\omega^{+/-} = \omega_{ref}^{+/-} - \omega_o^{+/-} \tag{7}$$

$$\Delta V^{+/-} = V_{ref}^{+/-} - V_o^{+/-} \tag{8}$$

$$\Delta V_{mg}^{+/-} = V_g^{+/-} - V_o^{+/-} \tag{9}$$

$$\Delta\omega_{mg}^{+/-} = \omega_g^{+/-} - \omega_o^{+/-} \tag{10}$$

where $\omega_o^{+/-}$ are the detected positive/negative sequence angular frequency of GFMER; $\omega_g^{+/-}$ are the detected positive/negative sequence angular frequency of grid. It should be noted that the detection of GFMER output frequency and grid frequency is also based on DSOGI [25].

2) Power Calculation Module: The primary control module lacks the capability to adjust the power reference value during asymmetrical grid voltage sags, resulting in voltage deviations even after the operation. Additionally, the DC/AC converter needs to possess dynamic support capability. To address these issues, a power calculation module is developed based on the primary droop module, as shown in Fig. 4. This module calculates the suitable power reference value based on the severity of asymmetrical voltage sags, enabling dynamic adjustment of the power reference value.

By coordinate transformation, both the voltage and current at the PCC point can be expressed by the positive and negative sequence components in $\alpha\beta$ coordinates, with the voltage expressed as shown in (11) and the current expressed as shown in (12).

$$\begin{aligned} v_o &= v_o^+ + v_o^- = \begin{bmatrix} u_{o\alpha} \\ u_{o\beta} \end{bmatrix} \\ &= \begin{bmatrix} V_o^+\cos(\omega t+\varphi^+) + V_o^-\cos(\omega t+\varphi^-) \\ V_o^+\sin(\omega t+\varphi^+) + V_o^-\sin(\omega t+\varphi^-) \end{bmatrix} \end{aligned} \tag{11}$$

$$\begin{aligned} i_g &= i_g^+ + i_g^- \\ &= \begin{bmatrix} I_{gP}^+\cos(\omega t+\varphi^+) + I_{gP}^-\cos(\omega t+\varphi^-) \\ I_{gP}^+\sin(\omega t+\varphi^+) + I_{gP}^-\sin(\omega t+\varphi^-) \end{bmatrix} \\ &\quad + \begin{bmatrix} -I_{gQ}^+\sin(\omega t+\varphi^+) - I_{gQ}^-\sin(\omega t+\varphi^-) \\ I_{gQ}^+\cos(\omega t+\varphi^+) + I_{gQ}^-\cos(\omega t+\varphi^-) \end{bmatrix} \end{aligned} \tag{12}$$

where $v_o^{+/-}$ are the positive/negative sequence voltage respectively; $i_g^{+/-}$ are the positive/negative sequence current respectively. $V_o^{+/-}$ are the positive/negative sequence voltage amplitude of PCC, $I_{gP}^{+/-}$ and $I_{gQ}^{+/-}$ are the positive/negative sequence amplitudes of active and reactive current, respectively; $\varphi^{+/-}$ are the positive/negative sequence voltage phasor phase angle; ω is the angular frequency.

Then, transforming $V_o^{+/-}$, $I_{gP}^{+/-}$ and $I_{gQ}^{+/-}$ from the (11) and (12) into the *d*-*q* axis, can be obtained as:

$$V_{od}^{+/-} = V_o^{+/-} \tag{13}$$

$$V_{oq}^{+/-} = 0 \tag{14}$$

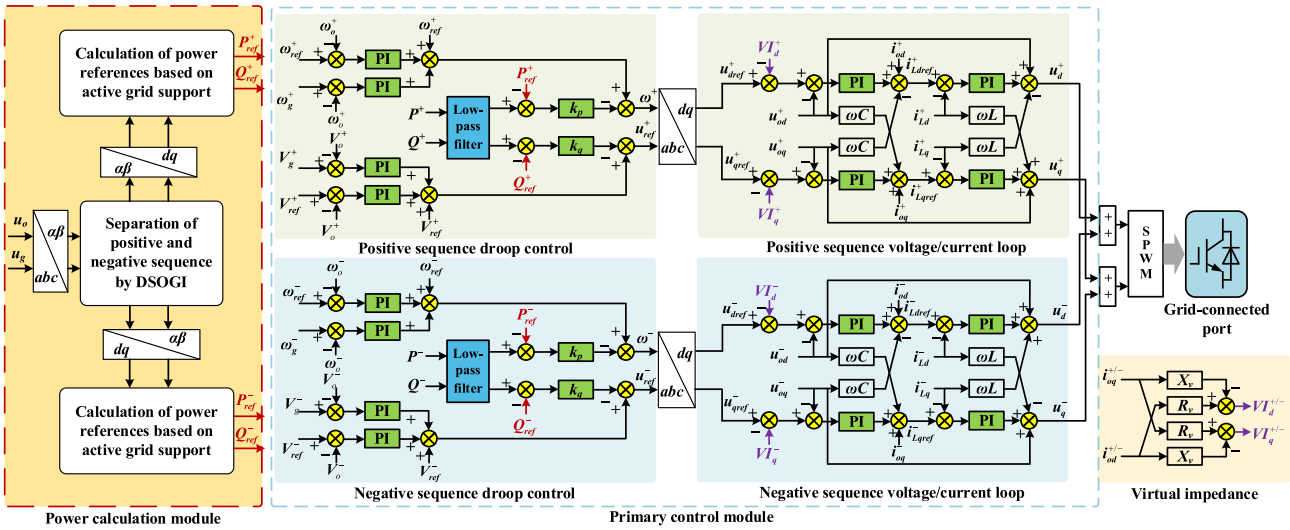

Fig. 4. Control strategy of DC/AC converter.

$$I_{gd}^{+/-} = I_{gP}^{+/-} \tag{15}$$

$$I_{gq}^{+/-} = I_{gQ}^{+/-} \tag{16}$$

The relationship between the PCC voltage and the grid voltage in the $\alpha\beta$ coordinate system is:

$$v_{o\alpha} = v_{g\_\alpha} + L_g \frac{di_{g\alpha}}{dt} + R_g i_{g\alpha} \tag{17}$$

$$v_{o\beta} = v_{g\_\beta} + L_g \frac{di_{g\beta}}{dt} + R_g i_{g\beta} \tag{18}$$

Then, using (11) and (12) and (15)–(18), the equation of the voltage support would be [29]:

$$V_o^+ - V_g^+ = I_{gd}^+ R_g + I_{gq}^+ \omega L_g \tag{19}$$

$$V_o^- - V_g^- = I_{gd}^- R_g + I_{gq}^- \omega L_g \tag{20}$$

where $V_g^{+/-}$ are the positive/negative sequence voltage amplitudes on the grid respectively.

As can be seen from (19) and (20), if the low-voltage power grid is considered to be resistive rather than pure inductive, the influence of the active current component on the voltage support of the power grid cannot be ignored.

By substituting the positive/negative sequence voltage reference values ($V_{ref}^{+/-}$) into the above equation, the total reference value of positive and negative sequence current ($I_{sd}^{+/-}$ and $I_{sq}^{+/-}$) required to proactively support the grid can be obtained as:

$$I_{sd}^+ = \frac{V_{ref}^+ - V_g^+}{X_g^2 + R_g^2} R_g \tag{21}$$

$$I_{sq}^+ = \frac{V_{ref}^+ - V_g^+}{X_g^2 + R_g^2} \omega L_g \tag{22}$$

$$I_{sd}^- = \frac{V_g^- - V_{ref}^-}{X_g^2 + R_g^2} R_g \tag{23}$$

$$I_{sq}^- = \frac{V_{ref}^- - V_g^-}{X_g^2 + R_g^2} \omega L_g \tag{24}$$

It should be noted that in grid-forming mode, the system does not need to support the grid, so the support current is 0 during grid-forming mode. Considering the AC load current and (21)–(24), the total reference current is assigned according to each GFMER capacity, and the initial current reference value of each GFMER ($I_{okd}^{ini+/-}$ and $I_{okq}^{ini+/-}$) can be obtained as:

$$I_{okd}^{ini+} = \frac{S_{nk}}{S_{n1} + \cdots + S_{nn}} \left(I_{loadd} + \frac{V_{ref}^+ - V_g^+}{X_g^2 + R_g^2} R_g \right) \tag{25}$$

$$I_{okq}^{ini+} = \frac{S_{nk}}{S_{n1} + \cdots + S_{nn}} \left(I_{loadq} + \frac{V_{ref}^+ - V_g^+}{X_g^2 + R_g^2} \omega L_g \right) \tag{26}$$

$$I_{okd}^{ini-} = \frac{S_{nk}}{S_{n1} + \cdots + S_{nn}} \left(\frac{V_g^- - V_{ref}^-}{X_g^2 + R_g^2} R_g \right) \tag{27}$$

$$I_{okq}^{ini-} = \frac{S_{nk}}{S_{n1} + \cdots + S_{nn}} \left(\frac{V_{ref}^- - V_g^-}{X_g^2 + R_g^2} \omega L_g \right) \tag{28}$$

where I_{loadd} and I_{loadq} are the load current in the d-q axis; S_{n1}, S_{nk} and S_{nn} are the capacity of *1*th, *k*th and *n*th converter.

The positive/negative sequence active/reactive power output ($P^{+/-}$ and $Q^{+/-}$) by GFMERs are calculated by using a first order low pass filter as follows [30]:

$$P^+ = \frac{3\omega_c}{2(s+\omega_c)} \left(V_{gd}^+ I_{od}^+ + V_{gq}^+ I_{oq}^+ \right) \tag{29}$$

$$Q^+ = \frac{3\omega_c}{2(s+\omega_c)} \left(V_{gq}^+ I_{od}^+ - V_{gd}^+ I_{oq}^+ \right) \tag{30}$$

$$P^- = \frac{3\omega_c}{2(s+\omega_c)} \left(V_{gd}^- I_{od}^- + V_{gq}^- I_{oq}^- \right) \tag{31}$$

$$Q^- = \frac{3\omega_c}{2(s+\omega_c)}\left(V_{gq}^- I_{od}^- - V_{gd}^- I_{oq}^-\right) \tag{32}$$

where ω_c is the cut-off angular frequency of the low-pass filters.

By substituting the current reference values in (25)–(28) into (29)–(32), the positive/negative sequence active/reactive power initial reference values of droop control ($P_{ini}^{+/-}$ and $Q_{ini}^{+/-}$) can be obtained. Note that the final reference values ($P_{ref}^{+/-}$ and $Q_{ref}^{+/-}$) needs to be obtained from the upper-layer controller. Then, the calculated reference values are sent afterwards to the primary control module. By combining the two control modules, the proposed droop control enables GFMER to provide accurate support to the grid.

It should be noted that the calculation of reference power depends on the grid impedance parameters R_g and L_g. The unavailability or inaccuracy of these values will impact the performance of the control system. However, several techniques have been proposed for estimating grid impedance by means of grid-connected inverters. These techniques can be mainly divided into three classifications: passive [31], active [32], [33], and hybrid [34], [35]. Among them, Reference [35] introduces a multi-inverter impedance estimation method based on event-triggered mechanism, with experimental results demonstrating its accuracy. This approach estimates impedance based on changes in the inverter's output power, including active power and reactive power, making it suitable for the proposed parallel grid-forming GFMER system in this paper. Therefore, the method proposed in [35] is employed to obtain the grid impedance parameters if they are not explicitly available. Owing to the effect of the event-triggered mechanism, when the grid impedance changes, it will be automatically estimated again.

IV. The Upper-Layer Controller

The upper-layer controller is a supervisory control system responsible for managing the overall operation of the GFMER, as shown in Fig. 5. The main functions are as follows: 1) performing internal energy management and calculating the exchange power between the GFMER and the grid; 2) proactively regulating voltage imbalances and deviations on the AC grid side to the maximum extent possible; and 3) actively switching operation modes in response to varying degrees of grid sags. Firstly, the variables are initialized and the monitored data is processed. Secondly, the operating modes of the PV and BESU are determined according to the internal energy management strategy. Then, the operating mode is actively switched according to the depth of grid voltage sag. The power allocation module is incorporated in grid-connected mode and transient support mode to optimize grid support. Finally, the instructions are sent to the lower-layer controller.

A. Data Processing

Initially, initialize the variables, including the rated capacity (S_n). Subsequently, monitor the real-time values of voltages and currents as indicated by the red markers in Fig. 1, and the real-time SoC of BESU. Finally, process the measured data to compute the power of the PV, BESU, local load and grid-connected ports.

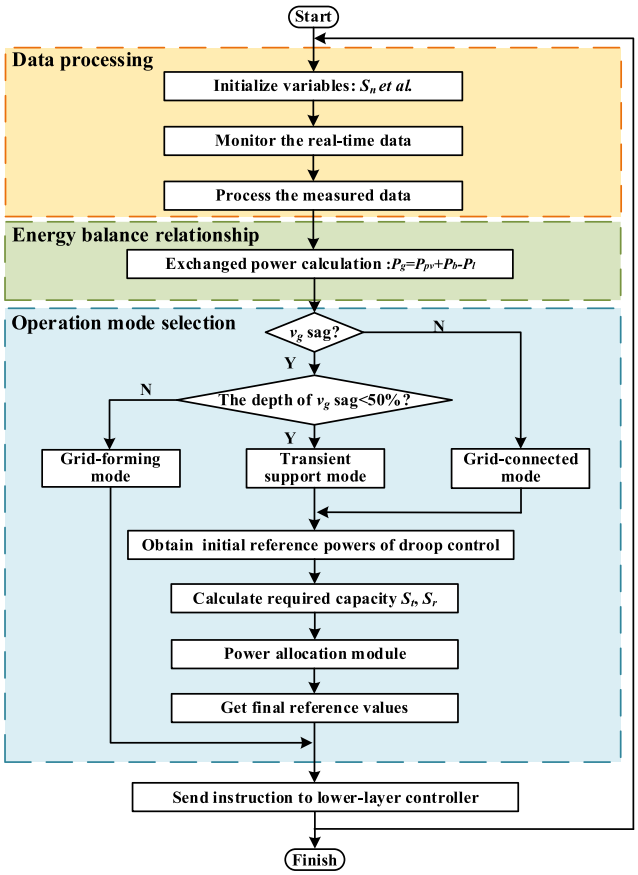

Fig. 5. The flow chart of upper-layer controller.

B. Energy Balance Relationship

The energy flow in the GFMER is governed by its internal power balance mechanism, which ensures stable operation and effective interaction with the grid. The energy balance relationship inside the energy router is shown as:

$$P_g = P_{pv} + P_b - P_l \tag{33}$$

where P_g is the power exchanged between the GFMER and the grid; P_l is the DC load power inside the energy router; P_{pv} is the output power of the PV system; and P_b is the output power of the BESU. This energy balance equation provides a fundamental understanding of the dynamic power flow within the energy router, which calculates power based on real-time data and operational requirements. Moreover, the calculated P_g serves as an essential parameter for the power allocation module.

C. Mode Classification

The proposed GFMER operates in three distinct modes: grid-connected mode, transient support mode, and grid-forming mode. These modes enable power exchange, proactive grid support, and local load optimization, respectively, ensuring reliable and efficient power distribution.

1) *Grid-connected mode:* The GFMER operates in grid-connected mode when the grid is operating normally. In this mode, GFMER not only exchange power with the grid, bus also perform steady-state support to improve the power quality of the grid.
2) *Transient support mode:* When the voltage sag in the grid is detected and the depth of sag is less than 50%, GFMER will operate in transient support mode. In this mode, the GFMER responds rapidly by supplying specified positive/negative sequence active/reactive power to proactively support the grid.
3) *Grid-forming mode:* If the voltage sag in the grid exceeds 50%, it is not possible to raise the voltage to the rated range due to the limitations of the GFMER capacity even with proactive support. To ensure premium operation of local AC and DC loads, the GFMER will be off-grid and operation in grid-forming mode. In this mode, the secondary amplitude and frequency control can reduce the amplitude and frequency deviation of the output voltage.

D. Power Allocation Module

A power allocation module is added to the grid-connected mode and the transient support mode. This module takes into account the requirements power for proactively support and redistributes the power inside the GFMER by dividing the power priority. In addition, due to the limited capacity of the GFMER, how to reasonably allocate the access power to maximize the support of the grid has become a challenge. Hence, the capacity of the GFMER is also fully considered. The reference power for droop control is further adjusted by the module to optimize support.

The proposed strategy prioritizes premium power supply and proactive voltage support as primary and secondary objectives, respectively, ranking the power output of each port accordingly. Among them, the power of the load output port is the highest level to ensure the quality of the load's power supply needs under any conditions. The allocation of active and reactive power to support the grid is prioritized at the second level to enhance active support capability in various scenarios. Finally, the exchange power between GFMER and power grid is set to third level.

The amount of the active and reactive power applied to support the voltage can be expressed as:

$$P_s = P_{ini}^{+} + P_{ini}^{-} \tag{34}$$

$$Q_s = Q_{ini}^{+} + Q_{ini}^{-} \tag{35}$$

where P_s and Q_s are the active and reactive power applied to support the voltage respectively.

The exchanged power P_g can be expressed as:

$$P_g = P_{out} + P_s \tag{36}$$

where P_{out} is the power delivered from the GFMER to the grid.

The total required capacity S_t and the voltage support required capacity S_r can be calculated as:

$$S_t = \sqrt{(P_{out} + P_s)^2 + Q_s^2} \tag{37}$$

$$S_r = \sqrt{{P_s}^2 + Q_s^2} \tag{38}$$

Based on the relationship between S_t, S_r and the rated capacity of the converter S_n, three scenarios can be divided as follows:

1) *Scenario 1:* When $S_t > S_n > S_r$, the total required capacity exceeds the converter's rated capacity, potentially causing overload. In order to ensure the effect of voltage support, the active and reactive reference power required for support will not change. The power delivered to the grid will be adjusted as:

$$P_{out} = \sqrt{S_n^2 - Q_s^2} - P_s \tag{39}$$

2) *Scenario 2:* When $S_t > S_r > S_n$, the converter needs to output more power to actively support the power grid. However, due to the capacity limitation of the converter, it is unable to provide the required power to the grid, so it is necessary to adjust the power reference value as:

$$P_{out} = 0 \tag{40}$$

$$P_{ref}^{+/-} = P_{ini}^{+/-} \frac{S_n}{S_r} \tag{41}$$

$$Q_{ref}^{+/-} = Q_{ini}^{+/-} \frac{S_n}{S_r} \tag{42}$$

3) *Scenario 3:* When $S_n > S_t > S_r$, the power required for active support is small, and the total required capacity is below the converter's rating. Therefore, no adjustments to the reference power are needed, and the final reference power remains equal to the initial value.

Combining (33) and (36), it can be obtained that P_{out} is influenced by P_{pv}. If P_{out} needs to be adjusted, the PV will operate in power-limited mode with a specific reference power (P_{limit}) issued by the upper-layer controller, which can be calculated as:

$$P_{\text{limit}} = P_{out} + P_s + P_l - P_b \tag{43}$$

V. Simulation Results

A two-parallel GFMER system connecting to the distribution grid is compiled based on MATLAB/Simulink in this paper. The major system parameters are given in Table I. Various GFMER operating modes are simulated to verify the effectiveness of the proposed control strategy in each mode.

A. Grid-Connected Simulation

The GFMER operates in grid-connected mode when the grid is operating normally. In this mode, GFMER not only exchanges power with the grid, but also perform steady-state support to improve the power quality of the grid. The irradiance in the grid-connected simulation fluctuates between 600–1000 W/m^2. The grid voltage deviation was set to 9% (with the grid still operating within the normal rated range) to verify the steady-state support capability of the GFMER.

As shown in Fig. 6(a), when the grid voltage deviation is 9%, the PCC voltage remains at 1.0 p.u. under the steady-state support of the GFMER, ensuring the reliability of the power supply to the AC loads. The power curves of one GFMER's PV, BESU, DC load, and DC/AC active and reactive power output

TABLE I
MAJOR PARAMETERS OF THE SYSTEM

Parameters	Symbol	Values
Distribution grid voltage	v_g	380 V
AC frequency	f_g	50 Hz
GFMER DC bus voltage	U_{bus}	750 V
BESU voltage	U_{Lb}	450 V
BESU capacity	S_{Lb}	20 Ah
Inductance of grid impedance	L_g	12 mH
Resistance of grid impedance	R_g	0.8 Ω
LCL filter in grid-connected port	L_{f1}, C_f, L_{f2}	12 mH, 10 μF, 0.6 mH
Capacity of grid-connected port	S_n	10 kVA
Maximum power of PV	P_{mpp}	30 kW
Local AC loads	$P_{l\text{-}AC}$	12 kW
DC loads of each GFMER	P_l	14 kW
Switching Frequency	f_s	10 kHz

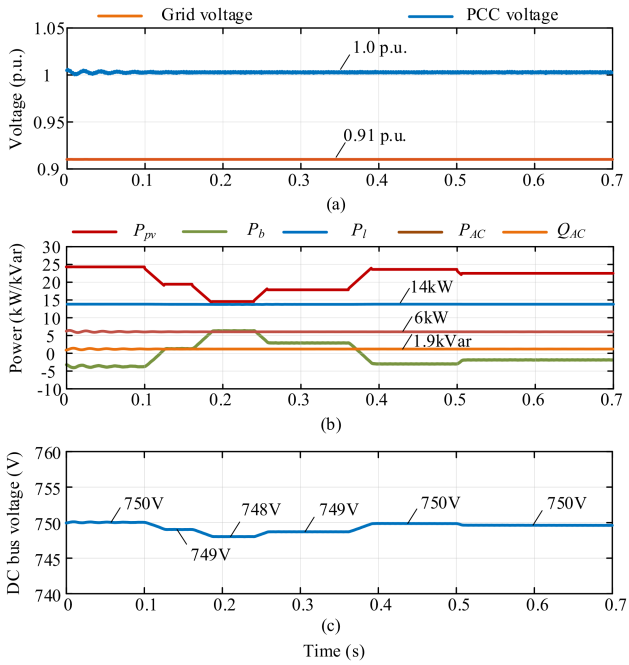

Fig. 6. Simulation results in grid-connected mode: (a) Frequency and (b) amplitude of PCC voltage.

are shown in Fig. 6(b). It is shown that the PV output power varies with the irradiance and the BESU outputs or absorbs power to maintain power balance. The DC load consistently consumes 14 kW of power. The DC/AC port outputs 6 kW of active power to meet the AC load demand, while also supplying 1.9 kVar of reactive power to support the PCC voltage. The DC bus voltage of a single GFMER is shown in Fig. 6(c). As the PV power fluctuates, the DC bus voltage undergoes slight variations, but the fluctuation amplitude does not exceed 5 V, ensuring the reliability of the power supply to the DC load.

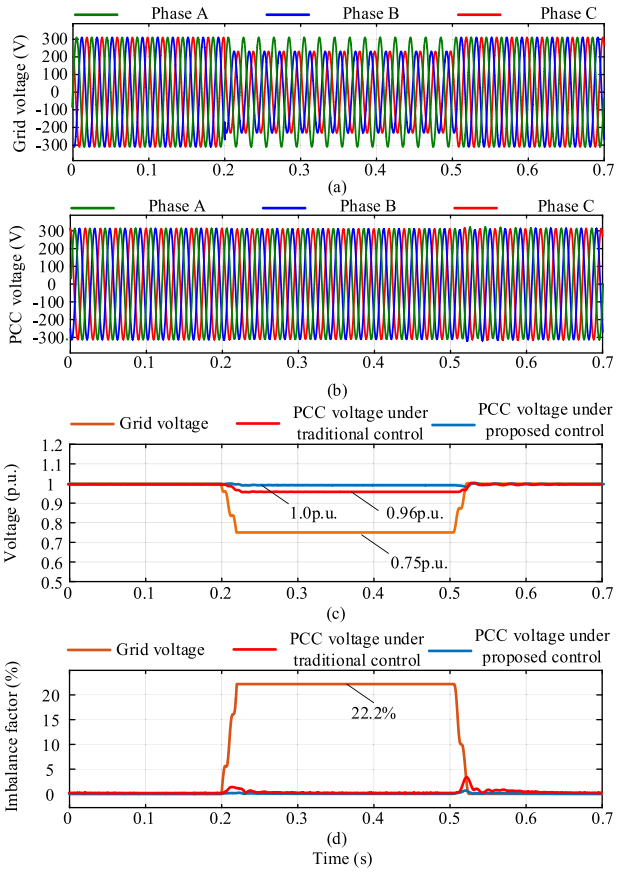

Fig. 7. Simulation results in 25% voltage sag: (a) Grid voltage, (b) PCC voltage, (c) voltage under different controls, and (d) imbalance factor under different controls.

B. Transient Support Simulation

The transient support mode is operated under grid connection. The irradiance in this simulation fluctuates between 600–1000 W/m^2. The proactive support performance of the proposed control is tested in the 25% two-phase voltage sag. As shown in Fig. 7(a), the phase voltage amplitude is 311 V under normal conditions, and the sag occurs at $t = 0.2$ s and clears at $t = 0.5$ s. The PCC voltage proactively supported by GFMER is shown in Fig. 7(b). It is obvious that the PCC voltage is increased to 311 V instantaneously during the grid voltage sag, and the grid voltage sag has little effect on it. To verify the improvements of the proposed control strategy, we compared it with the existing droop control with positive and negative sequence separation, as shown in Fig. 7(c) and (d). It can be observed that the GFMER using the proposed control strategy provides better support, as evidenced by the smaller voltage deviation and imbalance factor. Therefore, the GFMER can effectively support the PCC voltage and protect the AC sensitive loads from damage under the grid voltage sag.

The output power of GFMER 1 and GFMER 2 under grid voltage sag is shown in Fig. 8(a). It is clear that GFMERs can adaptively output the appropriate active/reactive power based on the depth of the voltage sag under the combined effect of the proposed droop control and power distribution modules, and the

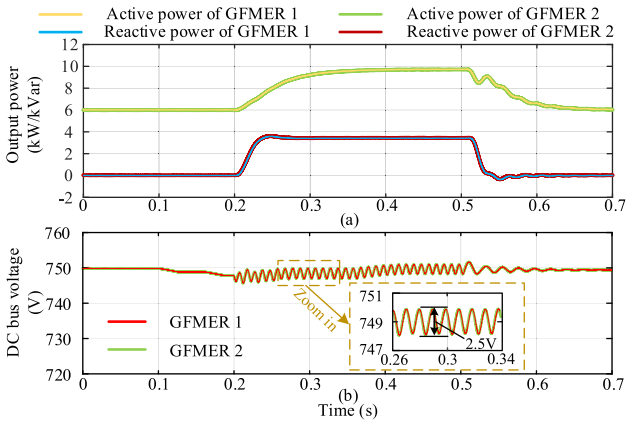

Fig. 8. Simulation results in 25% voltage sag: (a) GFMER output power, and (b) GFMER DC bus voltage.

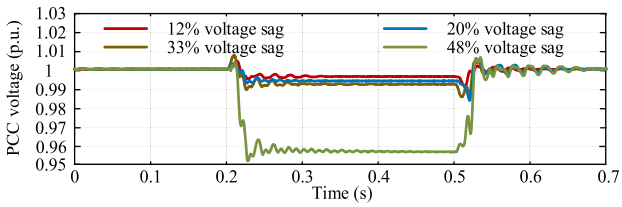

Fig. 9. PCC voltage in different grid voltage sags.

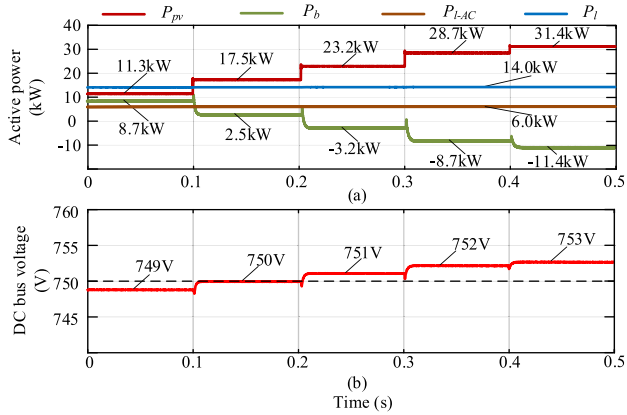

Fig. 10. Simulation results in grid-forming mode: (a) Power of PV, BESU and AC/DC loads, and (b) DC bus voltage.

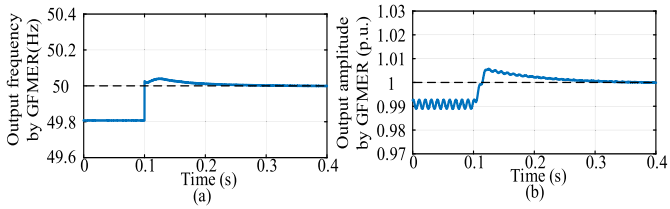

Fig. 11. Simulation results in grid-forming mode: (a) Secondary frequency control and (b) secondary amplitude control.

output power is well shared between the parallel GFMERs. It can be seen from Fig. 8(b) that under the condition of varying light irradiances and proactive support, DC bus voltage is maintained near 750 V to ensure the normal operation of DC load which verifies the effectiveness of the upper-layer controller in transient support mode. Due to the effect of negative-sequence components, the DC-side voltage will experience oscillations at the time of proactive support. However, the amplitude of the DC bus voltage oscillation is only 2.5 V, which has a negligible effect on the DC loads.

Finally, the performance of proactive support is tested under different grid voltage sags. As shown in Fig. 9, when the depth of grid voltage sag is 12%, 20%, and 33% respectively, the PCC voltage is supported to over 0.99 p.u. due to the power distribution module and the proposed droop control. In the case of 48% voltage sag, due to the large capacity required for support and the limited capacity of the converter, the power distribution module makes an appropriate reduction in the reference power, and the PCC voltage is supported to 0.96 p.u.

C. Grid-Forming Simulation

Due to the limited capacity of the converter, PCC voltage will not meet the load operation requirements even if it is proactively supported by GFMER when the grid voltage sags seriously. In this case, GFMER will operation in grid-forming mode. In this simulation scenario, the PV power increases every 0.1 s.

The active power curves of PV, BESU and AC/DC loads during grid-forming mode are shown in Fig. 10(a). With the gradual increase of PV power, BESU changes from charging state to discharging state and the charging and discharging power changes according to the PV power. During this period, both AC and DC loads operate stably. It can be seen from Fig. 10(b) that the DC bus voltage is always maintained around 750 V with a maximum deviation of only 3 V. The ability of secondary voltage amplitude and frequency control is verified, as shown in Fig. 11. Secondary control is added at $t = 0.1s$. It is clear that the proposed control strategy incorporates a secondary regulation in the droop control, which is able to reduce the frequency and amplitude deviation of the output AC voltage of the output AC voltage of the GFMER and optimize the power quality. The simulation results verify the energy management capability of the proposed control strategy in the grid-forming mode.

D. Mode-Switching Simulation

A simulation analysis was performed to evaluate the transition between grid-connected mode and grid-forming mode. Fig. 12 shows the simulation results of grid-connected pre-synchronization. The GFMER is connected to the grid at $t = 0.8s$. It is obvious that the voltage and frequency fluctuations are significantly reduced at the time of grid connection with pre-synchronization. The amplitude and frequency waveforms of PCC voltage during the GFMER switching from grid-connected mode to grid-forming mode are shown in Fig. 13. The GFMER operates in grid-forming mode at $t = 1.5s$. The fluctuations in the frequency and amplitude of the PCC voltage during switching are almost negligible.

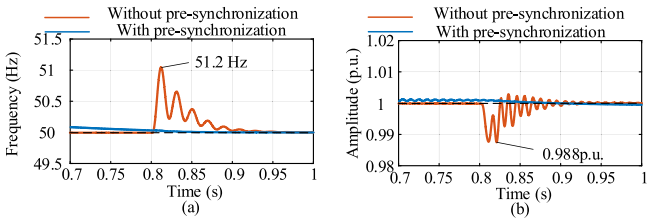

Fig. 12. Simulation results of transition from grid-forming to grid-connected mode: (a) Frequency and (b) amplitude of PCC voltage.

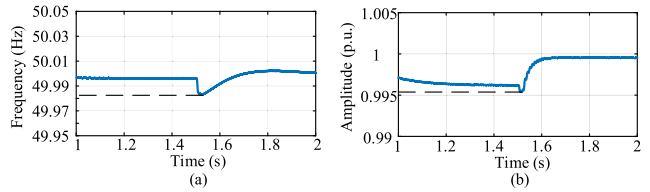

Fig. 13. Simulation results of transition from grid-connected to grid-forming mode: (a) Frequency and (b) amplitude of PCC voltage.

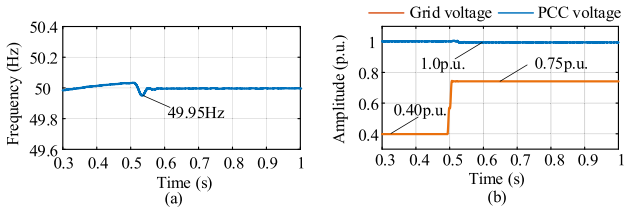

Fig. 14. Simulation results of transition from grid-forming to transient support mode: (a) Frequency and (b) amplitude of voltage.

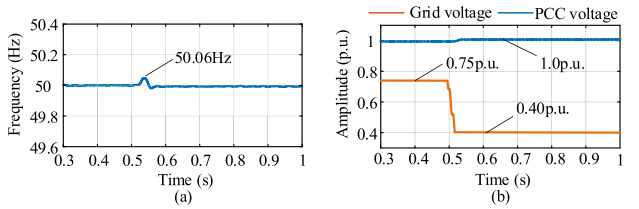

Fig. 15. Simulation results of transition from transient support mode to grid-forming mode: (a) Frequency and (b) amplitude of voltage.

Additionally, a simulation analysis was carried out for the transition between grid-forming mode and transient support mode. When the voltage sag depth decreases to below 50%, the GFMER transitions from grid-forming mode to transient support mode, as shown in Fig. 14. It can be observed that as the voltage sag depth reduces from 60% to 25% at $t = 0.5s$, the GFMER shifts to transient support mode to stabilize the PCC voltage. During this transition, both the frequency and amplitude fluctuations of the PCC voltage are minimal. Conversely, when the voltage sag depth exceeds 50%, the GFMER switches back from transient support mode to grid-forming mode to ensure reliable power supply to the load, as depicted in Fig. 15. The results indicate that the PCC frequency fluctuation during this transition is less than 0.1 Hz, and the voltage amplitude remains almost constant.

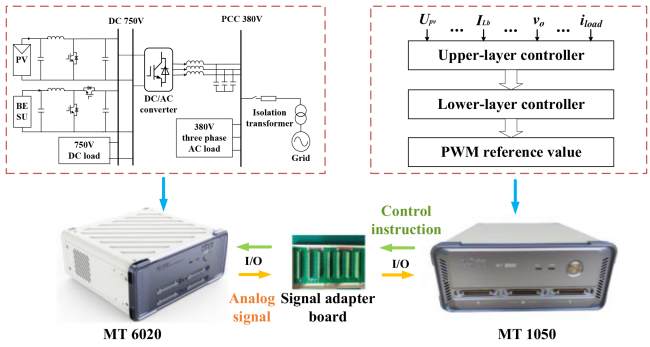

Fig. 16. Hardware platform of HIL experiment.

It should be noted that the switching between grid-connected mode and transient support mode can be validated in Fig. 7, so further analysis will not be repeated here. The simulation results clearly demonstrate that the proposed GFMER can seamlessly switch between different operating modes.

VI. Experimental Results

A GFMER system connected to the distribution network is implemented on the StarSim CHIL platform. The system parameters are shown in Table I and the only difference is that the local AC loads changes to 6 kW. The main circuit was simulated in MT 6020 simulator with a time step of 1 μs. The hierarchical proactive control of the GFMER is implemented by the MT1050 rapid control prototype (RCP) with a time step of 10 μs. Due to the limited number of I/O ports, the proposed control strategy is implemented in only one GFMER. However, all multiple GFMERs in parallel are based on the same control strategy and the same parameters, and if one GFMER scenario can be verified, multiple GFMERs scenarios can also be verified. The CHIL platform diagram is shown in Fig. 16.

The transient support mode is operated under grid connection. If the transient support capability can be verified, the steady state support capability in grid-connected mode can also be verified. Therefore, this experiment mainly verifies the transient support capability. The experimental results of GFMER transient proactive support are shown in Fig. 17. The 25% two-phase voltage sag occurred in the grid at 0.44 s with a duration of 1s, as shown in Fig. 17(a). The PCC voltage supported by GFMER is shown in Fig. 17(b). Comparing Fig. 17(a) and (b), the PCC voltage is supported and becomes more balanced due to the positive/negative sequence power injected. Fig. 17(c) shows the DC bus voltage inside the GFMER during the support period. It is clear that the voltage oscillations during the support period are only 10 V, which proves the balance of GFMER's internal power.

The experimental results of grid-forming mode are shown in Fig. 18. Fig. 18(a) shows the output power of GFMER in grid-forming mode. Obviously, in grid-forming mode, GFMER can precisely and stably output power to meet AC load demands. The internal DC bus voltage of GFMER is shown in Fig. 18(b). It

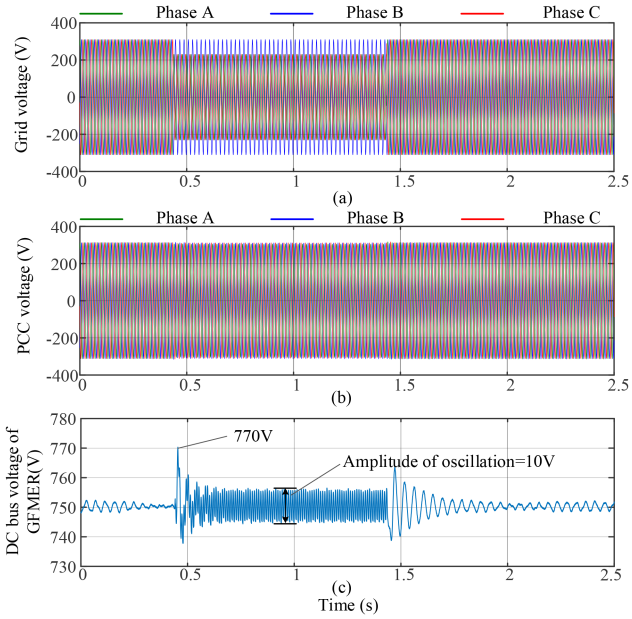

Fig. 17. The experimental results of GFMER transient proactive support: (a) Grid voltage; (b) PCC voltage; (c) output power of GFMER; and (d) DC bus voltage of GFMER.

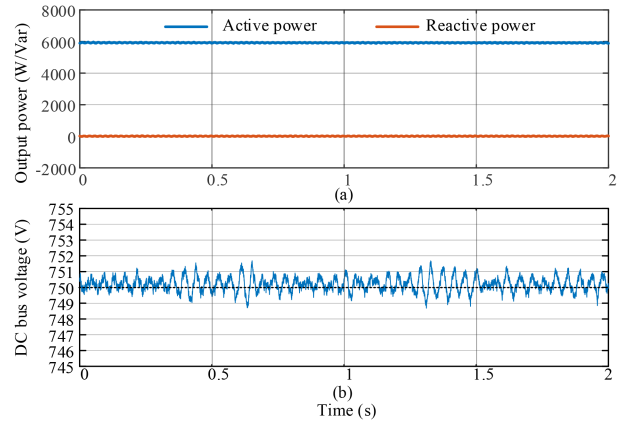

Fig. 18. The experimental results of grid-forming mode: (a) Output power of GFMER and (b) DC bus voltage of GFMER.

is obvious that the DC bus voltage is always maintained at 750 V, and the maximum oscillation amplitude does not exceed 3 V.

When GFMER switches between grid-connected and grid-forming operations, the PCC voltage is shown in Fig. 19. GFMER was connected to the grid at 0.67 s and switched to grid-forming operation at 2.56 s. It is obvious that the voltage does not fluctuate in the instant of mode switching, which verifies that the proposed GFMER can smoothly switch the operating mode.

VII. Conclusion

For the demand of high power quality requirements of industrial microgrids, this paper proposes a GFMER with a hierarchical cooperative control strategy supporting three operating

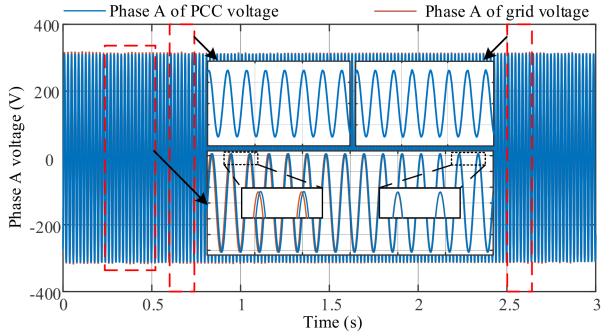

Fig. 19. Phase A voltage during mode switching.

modes. The simulation and experimental results indicate that the GFMER achieves effective energy complementarity between solar and storage systems while stabilizing the DC bus voltage and maintaining power balance under all conditions. Improved droop control enables more precise grid support during voltage sags, while the upper-layer power allocation module enhances dynamic support when needed. Secondary control and grid-connected pre-synchronization are added to the droop control, improving the power supply quality of GFMER in grid-forming mode and mode switching. The proposed GFMER can enhance power supply reliability and quality in industrial microgrids, particularly under varying grid conditions, which are crucial for industrial applications. Since current research does not consider external devices or multi-bus systems, future research will focus on scaling the GFMER system to larger and more complex microgrid networks, as well as addressing challenges related to device coordination and performance optimization in multi-bus configurations.

References

[1] S.-Y. Chen and C.-H. Chang, "Optimal power flows control for home energy management with renewable energy and energy storage systems," *IEEE Trans. Energy Convers.*, vol. 38, no. 1, pp. 218–229, Mar. 2023.

[2] N. Saxena, I. Hussain, B. Singh, and A. L. Vyas, "Implementation of a grid-integrated PV-battery system for residential and electrical vehicle applications," *IEEE Trans. Ind. Electron.*, vol. 65, no. 8, pp. 6592–6601, Aug. 2018.

[3] X. Quan et al., "Photovoltaic synchronous generator: Architecture and control strategy for a grid-forming PV energy system," *IEEE J. Emerg. Sel. Top. Power Electron.*, vol. 8, no. 2, pp. 936–948, Jun. 2020.

[4] J. Chen et al., "Distributed control of multi-functional grid-tied inverters for power quality improvement," *IEEE Trans. Circuits Syst. I, Reg. Papers*, vol. 68, no. 2, pp. 918–928, Feb. 2021.

[5] M. Gao, K. Wang, and L. He, "Probabilistic model checking and scheduling implementation of an energy router system in energy internet for green cities," *IEEE Trans. Ind. Inform.*, vol. 14, no. 4, pp. 1501–1510, Apr. 2018.

[6] L. Wang, H. Wang, M. Fu, J. Liang, and Y. Liu, "A three-port energy router for grid-tied PV generation systems with optimized control methods," *IEEE Trans. Power Electron.*, vol. 38, no. 1, pp. 1218–1231, Jan. 2023.

[7] R. Chen, Y. Yang, and T. Jin, "A hierarchical coordinated control strategy based on multi-port energy router of urban rail transit," *Protection Control Modern Power Syst.*, vol. 7, no. 2, pp. 1–12, Apr. 2022.

[8] P. Li, W. Sheng, Q. Duan, Z. Li, C. Zhu, and X. Zhang, "A Lyapunov optimization-based energy management strategy for energy hub with energy router," *IEEE Trans. Smart Grid*, vol. 11, no. 6, pp. 4860–4870, Nov. 2020.

[9] B. Liu, Y. Peng, J. Xu, C. Mao, D. Wang, and Q. Duan, "Design and implementation of multiport energy routers toward future energy internet," *IEEE Trans. Ind. Appl.*, vol. 57, no. 3, pp. 1945–1957, May/Jun. 2021.

[10] R. Wang, S. Jiang, D. Ma, Q. Sun, H. Zhang, and P. Wang, "The energy management of multiport energy router in smart home," *IEEE Trans. Consum. Electron.*, vol. 68, no. 4, pp. 344–353, Nov. 2022.
[11] A. Karbozov, M. G. Majumder, H. S. Krishnamoorthy, and K. Rajashekara, "Triple active bridge based multiport energy router for subsea – renewable interconnection," *IEEE Trans. Ind. Appl.*, vol. 59, no. 4, pp. 4528–4538, Jul./Aug. 2023.
[12] A. Datta, R. Sarker, and I. Hazarika, "An efficient technique using modified *p–q* theory for controlling power flow in a single-stage single-phase grid-connected PV system," *IEEE Trans. Ind. Inform.*, vol. 15, no. 8, pp. 4635–4645, Aug. 2019.
[13] M. Rajeev and V. Agarwal, "Low voltage ride-through capability of a novel grid connected inverter suitable for transformer-less solar PV–grid interface," *IEEE Trans. Ind. Appl.*, vol. 56, no. 3, pp. 2799–2806, May/Jun. 2020.
[14] R. Rai and B. Singh, "Converter control during low voltage ride through operation for grid-interfaced solar PV battery assisted system," *IEEE Trans. Ind. Electron.*, vol. 70, no. 9, pp. 9181–9191, Sep. 2023.
[15] E. Afshari et al., "Control strategy for three-phase grid-connected PV inverters enabling current limitation under unbalanced faults," *IEEE Trans. Ind. Electron.*, vol. 64, no. 11, pp. 8908–8918, Nov. 2017.
[16] H. Khan, S. J. Chacko, B. G. Fernandes, and A. Kulkarni, "Reliable and effective ride-through controller operation for smart PV systems connected to LV distribution grid under abnormal voltages," *IEEE J. Emerg. Sel. Top. Power Electron.*, vol. 8, no. 3, pp. 2371–2384, Sep. 2020.
[17] X. Zhao, J. M. Guerrero, M. Savaghebi, J. C. Vasquez, X. Wu, and K. Sun, "Low-voltage ride-through operation of power converters in grid-interactive microgrids by using negative-sequence droop control," *IEEE Trans. Power Electron.*, vol. 32, no. 4, pp. 3128–3142, Apr. 2017.
[18] C. Li, X. Liu, K. Sun, Y. Cao, F. Ma, and B. Zhou, "A hybrid control strategy to support voltage in industrial active distribution networks," *IEEE Trans. Power Del.*, vol. 33, no. 6, pp. 2590–2602, Dec. 2018.
[19] X. Cui, Y. Liu, D. Yuan, T. Jin, and M. A. Mohamed, "A hierarchical coordinated control strategy for power quality improvement in energy router integrated active distribution networks," *Sustainability*, vol. 15, no. 3, pp. 2655–2674, Feb. 2023.
[20] S. Zhao, Z. Wang, J. Umuhoza, A. Mantooth, Y. Zhao, and C. Farnell, "Distributed power quality enhancement using residential power routers," in *Proc. IEEE Appl. Power Electron. Conf. Expo.*, 2018, pp. 513–520.
[21] IEC standard voltages, IEC 60038:2009, International Electrotechnical Commission, Geneva, Switzerland, pp. 1–26, 2009.
[22] A. Sangwongwanich, Y. Yang, and F. Blaabjerg, "High-performance constant power generation in grid-connected PV systems," *IEEE Trans. Power Electron.*, vol. 31, no. 3, pp. 1822–1825, Mar. 2016.
[23] H. Akagi, Y. Kanazawa, and A. Nabae, "Instantaneous reactive power compensators comprising switching devices without energy storage components," *IEEE Trans. Ind. Appl.*, vol. TIA-20, no. 3, pp. 625–630, May 1984.
[24] M. Islam, M. Nadarajah, and M. J. Hossain, "A grid-support strategy with PV units to boost short-term voltage stability under asymmetrical faults," *IEEE Trans. Power Syst.*, vol. 35, no. 2, pp. 1120–1131, Mar. 2020.
[25] B. Hoepfner and R. Vick, "A three-phase frequency-fixed DSOGI-PLL with low computational effort," *IEEE Access*, vol. 11, pp. 34932–34941, 2023.
[26] J. M. Guerrero, J. Matas, L. G. de Vicuna, M. Castilla, and J. Miret, "Decentralized control for parallel operation of distributed generation inverters using resistive output impedance," *IEEE Trans. Ind. Electron.*, vol. 54, no. 2, pp. 994–1004, Apr. 2007.
[27] Y. C. C. Wong, C. S. Lim, M. D. Rotaru, A. Cruden, and X. Kong, "Consensus virtual output impedance control based on the novel droop equivalent impedance concept for a multi-bus radial microgrid," *IEEE Trans. Energy Convers.*, vol. 35, no. 2, pp. 1078–1087, Jun. 2020.
[28] Q. Shafiee, J. M. Guerrero, and J. C. Vasquez, "Distributed secondary control for islanded microgrids—A novel approach," *IEEE Trans. Power Electron.*, vol. 29, no. 2, pp. 1018–1031, Feb. 2014.
[29] J. Jia, G. Yang, and A. H. Nielsen, "A review on grid-connected converter control for short-circuit power provision under grid unbalanced faults," *IEEE Trans. Power Del.*, vol. 33, no. 2, pp. 649–661, Apr. 2018.
[30] A. Camacho, M. Castilla, J. Miret, A. Borrell, and L. G. de Vicuña, "Active and reactive power strategies with peak current limitation for distributed generation inverters during unbalanced grid faults," *IEEE Trans. Ind. Electron.*, vol. 62, no. 3, pp. 1515–1525, Mar. 2015.
[31] N. Hoffmann and F. W. Fuchs, "Minimal invasive equivalent grid impedance estimation in inductive–resistive power networks using extended Kalman filter," *IEEE Trans. Power Electron.*, vol. 29, no. 2, pp. 631–641, Feb. 2014.
[32] N. Mohammed, M. Ciobotaru, and G. Town, "An improved grid impedance estimation technique under unbalanced voltage conditions," in *Proc. IEEE PES Innov. Smart Grid Technol. Europe*, 2019, pp. 1–5.
[33] M. Ciobotaru, R. Teodorescu, and F. Blaabjerg, "On-line grid impedance estimation based on harmonic injection for grid-connected PV inverter," in *Proc. IEEE Int. Symp. Ind. Electron.*, 2007, pp. 2437–2442.
[34] P. García, M. Sumner, Á. Navarro-Rodríguez, J. M. Guerrero, and J. García, "Observer-based pulsed signal injection for grid impedance estimation in three-phase systems," *IEEE Trans. Ind. Electron.*, vol. 65, no. 10, pp. 7888–7899, Oct. 2018.
[35] N. Mohammed, T. Kerekes, and M. Ciobotaru, "Communication-free equivalent grid impedance estimation technique for multi-inverter systems," *IEEE Trans. Ind. Electron.*, vol. 70, no. 2, pp. 1542–1552, Feb. 2023.

Zixuan Zheng (Member, IEEE) received the B.S. and Ph.D. degrees in electrical engineering and its automation from Sichuan University, Chengdu, China, in 2012 and 2017, respectively. He is currently an Associate Professor with the College of Electrical Engineering, Sichuan University. His research interests include power quality, operation, and control of distributed energy resources.

Shijie Li received the B.S. degree from the College of New Energy, China University of Petroleum, Qingdao, China, in 2023. He is currently working toward the M.S. degree with the College of Electrical Engineering, Sichuan University, Chengdu, China. His research interests include control of energy storage systems and its applications in AC/DC microgrids.

Chunjun Huang (Member, IEEE) received the B.S. and M.S. degrees in electrical engineering from Sichuan University, Chengdu, China, in 2017 and 2020, respectively, and the Ph.D. degree from the Department of Wind and Energy Systems, Technical University of Denmark, Roskilde, Denmark. He is currently with the Department of Electrical Sustainable Energy, Delft University of Technology, Delft, The Netherlands. His research interests include power-to-hydrogen technologies, grid-scale alkaline electrolyzers, renewable energy-based green hydrogen, and integrated energy systems.

Yunzhu Chen received the M.S. and Ph.D. degrees in electrical engineering from Sichuan University, Chengdu, China, in 2018 and 2022, respectively. She is currently an Associate Researcher with the College of Electrical Engineering, Sichuan University. Her main research interests include voltage sag and premium power.

Junhao Ma received the B.S. degree from the College of Electrical Engineering, Taiyuan University of Technology, Taiyuan, China, in 2024. He is currently working toward the M.S. degree with the College of Electrical Engineering, Sichuan University, Chengdu, China. His research focuses on control of energy storage systems and its applications in AC/DC microgrids.

Mingshun Zhang received the B.S. and M.S. degrees from Sichuan Normal University, Chengdu, China, in 2020 and 2023, respectively. He is currently working toward the Ph.D. degree with the College of Electrical Engineering, Sichuan University, Chengdu. His research interests include DC microgrid, AC/DC hybrid microgrids, and superconducting magnetic energy storage.

Xianyong Xiao (Senior Member, IEEE) received the Ph.D. degree from Sichuan University, Chengdu, China, in 2010. He is currently a Professor and the Dean of the College of Electrical Engineering, Sichuan University. His research interests include power quality and its control, distribution system reliability, and environmentally friendly smart grids.

Jie Ren received the B.S. and Ph.D. degrees in electrical engineering and its automation from Sichuan University, Chengdu, China, in 2017 and 2022, respectively. She is currently a Lecturer with the College of Electrical Engineering, Sichuan University. Her research interests include renewable energy generation and fault ride through of the wind turbine generator.

Qiang Fu (Member, IEEE) received the Ph.D. degree from the School of Electrical and Electronic Engineering, North China Electric Power University, Beijing, China, in 2020. He is currently an Associate Research Fellow with the College of Electrical Engineering, Sichuan University, Chengdu, China. His main research interests include stability analysis and control of AC/DC hybrid power system considering renewable energy integration.